



Pharmaceutical nanotechnology

# Monoclonal antibody-targeted PEGylated liposome-ICG encapsulating doxorubicin as a potential theranostic agent



Neus Lozano <sup>a,1</sup>, Zahraa S. Al-Ahmady <sup>a,1</sup>, Nicolas S. Beziere <sup>b</sup>, Vasilis Ntziachristos <sup>b,\*\*</sup>, Kostas Kostarelos <sup>a,\*</sup>

<sup>a</sup> Nanomedicine Laboratory, Faculty of Medical & Human Sciences, University of Manchester, AV Hill Building, Manchester M13 9PT, United Kingdom

<sup>b</sup> Institute for Biological and Medical Imaging (IBMI), Technische Universität München and Helmholtz Zentrum München, Ingolstädter Landstrasse 1, 85764 Neuherberg, Germany

## ARTICLE INFO

## Article history:

Received 13 October 2014

Accepted 17 October 2014

Available online 23 October 2014

## Keywords:

Cancer nanotechnology

Optical imaging

Targeting

Photoacoustics

Nanomedicine

## ABSTRACT

Indocyanine green (ICG) is an FDA-approved, strongly photo-absorbent/fluorescent probe that has been incorporated into a clinically-relevant PEGylated liposome as a flexible optoacoustic contrast agent platform. This study describes the engineering of targeted PEGylated liposome-ICG using the anti-MUC-1 “humanized” monoclonal antibody (MoAb) hCTM01 as a tumour-specific theranostic system. We aimed to visualise non-invasively the tumour accumulation of these MoAb-targeted liposomes over time in tumour-bearing mice using multispectral optoacoustic tomography (MSOT). Preferential accumulation of targeted PEGylated liposome-ICG was studied after intravenous administration in comparison to non-targeted PEGylated liposome-ICG using both fast growing (4T1) and slow growing (HT-29) MUC-1 positive tumour models. Monitoring liposomal ICG in the tumour showed that both targeted and non-targeted liposome-ICG formulations preferentially accumulated into the tumour models studied. Rapid accumulation was observed for targeted liposomes at early time points mainly in the periphery of the tumour volume suggesting binding to available MUC-1 receptors. In contrast, non-targeted PEGylated liposomes showed accumulation at the centre of the tumour at later time points. In an attempt to take this a step further, we successfully encapsulated the anticancer drug, doxorubicin (DOX) into both targeted and non-targeted PEGylated liposome-ICG. The engineering of DOX-loaded targeted ICG liposome systems present a novel platform for combined tumour-specific therapy and diagnosis. This can open new possibilities in the design of advanced image-guided cancer therapeutics.

© 2014 Elsevier B.V. All rights reserved.

## 1. Introduction

Since the original description of phospholipid self-assembly into closed bilayer vesicles in aqueous media (Bangham and Horne, 1964) liposomes have received significant attention as drug delivery systems and made considerable contributions in various fields including clinical medicine (Al-Jamal and Kostarelos, 2011). Their versatility to cargo either hydrophilic (entrapped in the inner aqueous core) or hydrophobic (incorporated within the lipid bilayer) entities, combined with tuneable size and surface

properties have proven clinically useful (Al-Jamal et al., 2011; Sawant and Torchilin, 2010; Schwendener and Schott, 2010).

Liposomes have been engineered to circulate longer in the bloodstream and evade capture by the reticuloendothelial system, typically using polyethylene glycol (PEG) grafting on their outer surface (Gabizon et al., 1994). These surface-modified nanoscale vesicles have been applied to transport anti-neoplastic small molecules, such as doxorubicin (DOXIL<sup>®</sup>) and have been clinically used against various cancer indications (Barenholz, 2012; Eitan et al., 2014; Gabizon et al., 2012; Minisini et al., 2008; Tejada-Berges et al., 2002). PEGylated nanoparticles in general, including liposomes, have been described to preferentially accumulate within the interstitium of tissues with a leaky vascular bed through the enhanced permeation and retention (EPR) effect (Fang et al., 2011; Iyer et al., 2006; Maeda, 2012; Maeda et al., 2013). However, the accumulation of liposomes into the tumour is a highly heterogeneous process that varies between tumour models and consequently among patients (Jain and Stylianopoulos, 2010).

\* Corresponding author. Tel.: +44 161 275 1800.

\*\* Corresponding author. Tel.: +49 89 3187 3852.

E-mail addresses: [v.ntziachristos@tum.de](mailto:v.ntziachristos@tum.de) (V. Ntziachristos), [kostas.kostarelos@manchester.ac.uk](mailto:kostas.kostarelos@manchester.ac.uk) (K. Kostarelos).

<sup>1</sup> These authors contributed equally to this work.

In addition, the clinical potential of the EPR effect is not yet conclusive (Prabhakar et al., 2013), therefore, the development of image-guided drug delivery systems would be highly advantageous in order to determine spatially and temporally the optimum distribution of the liposomes into the pathological sites for both diagnostic and theranostic purposes.

Active targeting of liposomes, engineered with targeting ligands that bind specifically to overexpressed receptors at target diseased sites and cell populations, has also been a promising strategy to improve liposomal drug delivery (Allen, 2002; Kirpotin et al., 2006; Torchilin, 2008). PEGylated liposomes are more difficult to internalise within tumour cells *in vitro* and *in vivo* (Gabizon et al., 2010) and active targeting can be employed to achieve not only target cell recognition, but also specific binding and cellular uptake resulting in increased therapeutic potential (Mamot et al., 2005; Park et al., 2001). Targeted liposome internalisation within tumour cells may also lead to better drug bioavailability, especially for drugs acting against intracellular targets (Sapra and Allen, 2002). Kirpotin et al. showed that anti-HER2 targeted liposomes have improved intra-tumoural micro-distribution and cellular localisation compared to non-targeted anti-HER2 liposomes. A significant portion of HER2-targeted liposomes was observed within cancer cells, whereas, non-targeted liposomes were mainly found in stromal cells (Kirpotin et al., 2006). Similarly, transferrin-targeted oxaliplatin liposomes showed significant tumour growth control in comparison to non-targeted liposomes as a result of intracellular drug transport into the cytoplasm of colon 26 tumour cells by transferrin receptor-mediated internalisation (Suzuki et al., 2008).

Using recent advances in instrumentation, image reconstruction and spectral unmixing techniques, multispectral optoacoustic tomography (MSOT) is emerging as a potent modality for visualisation in nanomedicine (Ntziachristos and Razansky, 2010). Using spectral differentiation, MSOT can enable sensing of optical contrast signals in the absence of baseline measurements at high resolution. This is a unique combination of imaging features not available to other modalities that is ideally suited for sensing optical contrast in three dimensions. Intrinsic MSOT tissue contrast is attributed primarily to haemoglobin, melanin, water and lipids. Contrast enhancement can be achieved by metallic nanoparticles (most notably gold) and organic chromophores or fluorochromes. Organic fluorochromes, while preferred for labelling in preclinical and clinical optical imaging, are often not ideal as they typically lose their light absorbing properties following light exposure. We have recently developed a powerful *in vivo* MSOT contrast agent by incorporating the strong photo-absorbing probe indocyanine green (ICG) into PEGylated liposomes (Beziere et al., 2015), demonstrating enhanced optoacoustic imaging characteristics compared to gold nanorods (Bao et al., 2013; Herzog et al., 2012; Lozano et al., 2012) for the same number of nanoparticles injected.

Liposome systems labelled with ICG have been considered previously as fluorescent agents for subcutaneous or intradermal administration in the footpad region of healthy animals, mainly intended for lymph-node imaging using the IVIS or Maestro systems (Jeong et al., 2013; Proulx et al., 2010; Zhuang et al., 2012). However, none of those systems was designed with the intention for intravenous administration and systemic targeting and visualisation of tumours. Fluorescence imaging can be used for whole-body tracking of nanoparticle localisation, while MSOT imaging aims to visualise nanoparticles deeper within the tissue at high resolution and quantitatively, the latter not allowed by planar epi-illumination imaging.

The goal of the present study was to re-engineer the clinically-used PEGylated liposomes (the basis of the intravenous drug DOXIL<sup>®</sup>) by incorporating both optoacoustic imaging functionality

(using ICG) and a therapeutic agent (using the anticancer drug doxorubicin (DOX)). In addition, in order to improve the specificity of this system and tumour micro-distribution, surface conjugation of the “humanised” monoclonal antibody hCTM01 was performed to achieve tumour active targeting. hCTM01 is a high purity, clinical grade antibody that has been tested in human trials and has been proven very stable over long-term storage. hCTM01 Ab has been clinically evaluated by studying its biodistribution and therapeutic activity (Davies et al., 1997; Prinssen et al., 1998). In addition, hCTM01 antibody has shown great potential for the delivery of anticancer drugs and reduction of systemic toxicity due to its cellular internalising capacity, as in the case of the clinically tested hCTM01-calicheamicin immunoconjugate (Chan et al., 2003; Gillespie et al., 2000; Hinman et al., 1993).

The aim of the liposome systems engineered in this study was to build a biocompatible and biodegradable multi-functional vesicular platform, consisting of molecular components with clinically established toxicity profiles studied by *in vivo* MSOT imaging. The MoAb-targeted, PEGylated ICG liposomes were imaged using MSOT for non-invasive and longitudinal imaging of their distribution within the MUC-1 positive tumour models.

## 2. Materials and methods

### 2.1. Materials

$\text{l-}\alpha$ -Phosphatidylcholine, hydrogenated (HSPC) and 1,2-distearoyl-sn-glycero-3-phosphoethanolamine-*N*-[methoxy(polyethylene glycol)-2000] (DSPE-PEG<sub>2000</sub>) were kind gifts from Lipoid GmbH (Ludwigshafen, Germany). Cholesterol (Chol) and doxorubicin hydrochloride (DOX) were purchased from Sigma-Aldrich (UK). Indocyanine green (ICG) was obtained from Pulsion Medical Systems (Germany). Chloroform and methanol were purchased from Fisher Scientific (UK) and used as received. hCTM01; anti MUC-1 IgG mAb (150 kDa, Lot: 28735SC) was a kind gift from UCB (UK). McCoy's 5A (Modified) medium, Advanced RPMI 1640 (Roswell Park Memorial Institute) and  $\text{l-}$ glutamine (200 mM) were from Gibco Life Technologies (UK).

### 2.2. Culture of cancerous cell lines HT-29 and 4T1

4T1, murine breast cancer cells, and HT-29, human colon adenocarcinoma cells were grown in advanced RPMI 1640 and McCoy's 5A (modified) medium, respectively, supplemented with 10% FBS and 1% penicillin/streptomycin. Cells were cultured in 75 cm<sup>2</sup> sterile tissue culture flask (TPP, Switzerland) at 37 °C and 5% CO<sub>2</sub> level. Cells were passaged twice a week using trypsin-EDTA (Ca<sup>2+</sup> and Mg<sup>2+</sup> free) (Gibco) when reaching 80% confluency.

### 2.3. Cellular binding of anti-MUC-1 Ab

4T1 and HT-29 cancer cell line were selected after evaluation of their expression to MUC-1 antigen. 4T1 and HT-29 were grown on glass cover slip over night to reach confluency in 24 tissue culture well plate (corning USA) at 25,000 and 40,000 cells per well, respectively. Cells were then incubated with anti-MUC-1 antibody at 1  $\mu\text{g/ml}$  and 5  $\mu\text{g/ml}$  for 3 h at 37 °C. At the end of 3 h incubation cells were washed with PBS and fixed with PFA 4% (Thermo-scientific, UK) for 10–15 min at room temperature. Cells were then washed with PBS and permeabilised with 0.5% triton X-100 for 10 min and incubated with blocking solution composed of 4% goat serum and 3% BSA in PBS for 30 min. At the end of incubation cell were washed and incubated with anti-human Cy3-labelled secondary antibody at 1:220 dilution in blocking solution (2 h at room temperature protected from light). After 2 h, Cy3-labelled antibody was removed and cells were mounted using 3  $\mu\text{l}$

Vectashiled mounting medium with DAPI H-1200 (Vector Laboratories). Cells were then imaged using confocal laser scanning microscopy (CLSM) Zeiss LSM 710 (Oberkochen, Germany) at 405 nm and 514 nm laser excitation source, 410–585 nm output filter, and EC Plan-Apochromat 40x/1.3 oil to detect DAPI and Cy3 fluorescence signals, respectively.

#### 2.4. Preparation of liposomes

PEGylated liposome-ICG vesicles were prepared using the lipid film hydration method followed by freeze-fracture cycles and extrusion, as previously described (Beziere et al., 2015). Briefly, HSPC/Chol/DSPE-PEG<sub>2000</sub> (56.3:38.2:5.5) were dissolved in chloroform/methanol (4:1, v/v), and the organic solvents were evaporated under pressure using a rotary evaporator. The resulting thin lipid film was hydrated in 5% dextrose solution containing ICG. The dispersion was freeze-thawed in six cycles and then extruded. The unbound ICG was removed by using a de-salt spin column. The lipid concentration was determined by Stewart assay. The ICG content within the liposomes was measured by UV-vis spectrophotometer at 780 nm by dissolving the liposomes in DMSO and compared with the standard curve of ICG alone. For the PEGylated liposome-ICG-DOX, the DOX encapsulation was performed at the hydration step at the same time as the ICG in 5% dextrose and the unbound DOX was also removed by using the de-salt spin column. 1:20 DOX:total lipid mass ratio was used, and 5% was the encapsulation efficiency.

#### 2.5. Dynamic light scattering (DLS) and $\zeta$ -potential

Hydrodynamic diameter ( $\emptyset$ ) and electrophoretic mobility ( $\mu$ ) were measured at  $25 \pm 0.1$  °C by a Malvern Zetasizer unit, Nano ZS series HT. The hydrodynamic diameter is based on dynamic light scattering (DLS) technique in back scattering mode, at  $173^\circ$  and  $\lambda = 632.8$  nm. For  $\mu$  measurements the same dispersions were placed into U-shaped cuvettes, equipped with gold electrodes. The  $\zeta$ -potential is related to the  $\mu$  by Henry's equation valid in the Smoluchowski approximation, when the screening length is much smaller than the particle radius.

#### 2.6. UV-vis spectroscopy

The absorbance measurements were performed in a Varian Cary winUV 50 Bio spectrophotometer (USA). The optical density (OD) corresponds to the absorbance values by the diluted factor.

#### 2.7. Conjugation of hCTM01 antibody to PEGylated liposome-ICG with and without DOX

hCTM01 anti-MUC-1 antibody was first thiolated as previously described (Al-Ahmady et al., 2014) by mixing with Traut's reagent at Ab:Traut's reagent molar ratio of 1:20 for 1 h at room temperature with continuous stirring at concentration of 10 mg Ab/ml buffer, pH 8.0 (25 mM HEPES, 140 mM NaCl, 3 mM EDTA). Unreacted Traut's reagent was removed using Sephadex G50 column equilibrated with deoxygenated HBS (pH 7.4). The coupling reaction was run by mixing thiolated Ab with mal-DSPE-PEG<sub>2000</sub> micelles at 1:10 molar ratio in HBS (pH 7.4) overnight at room temperature. All above reactions were performed at oxygen free conditions. At the end of the reaction, any uncoupled mal-DSPE-PEG<sub>2000</sub> groups were blocked by mixing with cysteine HCl to a final concentration of 1 mM for 30 min (Loomis et al., 2010). Ab micelles were then concentrated by centrifugation using Viva spin 6 columns (Sartorius, fisher) at 9000 rpm for 10–12 min. Mal-DSPE-PEG<sub>2000</sub>-Ab micelles were then post inserted into preformed PEGylated liposome-ICG with and without DOX at Ab:lipids molar

ratios (1:500) by 1 h incubation at 60 °C. Targeted PEGylated liposome-ICG then separated from non-incorporated mal-DSPE-PEG<sub>2000</sub>-Ab micelles by using Sepharose CL-4B column in HBS (pH 7.4). In order to allow for direct comparison, PEGylated liposome-ICG and targeted PEGylated liposome-ICG liposomes with and without DOX were prepared following the same steps, except for the post-insertion process where HBS (pH 7.4) was used instead of mal-PEG<sub>2000</sub> Ab micelles. Post-insertion efficiency was determined by collecting elution fractions (1 ml each) and analysed spectrophotometrically for the presence of Ab (BCA protein assay, at 562 nm) (Yang et al., 2007) and liposomes (Stewart assay at 485 nm), using Cary 50 bio spectrophotometer (Agilent Technologies).

#### 2.8. Animal models for optoacoustic imaging experiments

All procedures involving animal experiments were approved by the Government of Upper Bavaria (ref. 55.2.1.54-2632-102-11). Two xenografted tumour models were employed one representative of a slow growing tumour, using HT-29 human adenocarcinoma cells and one representing rapid growth based on 4T1 murine breast cancer cells. 8 weeks old adult female Athymic Nude-Foxn1 mice (Harlan, Germany) were inoculated subcutaneously in the middle of the back in the region of the upper pelvis with cell suspensions (either  $0.8 \times 10^6$  4T1 (CRL-2539) cells or  $1.5 \times 10^6$  HT-29 (ATCC-HTB-38) cells) in 50  $\mu$ l PBS. Animals were imaged only after tumours reached a size of approximately 8 mm diameter.

#### 2.9. Multi-spectral optoacoustic tomography

All optoacoustic measurements were performed in a real-time whole-body mouse imaging MSOT system. An earlier version of the system was described previously (Buehler et al., 2010). Briefly, optical excitation was provided by a Q-switched Nd:YAG laser with a pulse duration of around 10 ns and a repetition rate of 10 Hz and a tuneable range of 680–900 nm. Light was homogeneously delivered to the sample using a fibre bundle split into 10 output arms. The emitted ultrasound signal was detected using a 64 element transducer array cylindrically focused and having a central frequency of 5 MHz, allowing acquisition of transverse plane images. The fibre bundle and transducer array were stationary, and the sample could be moved to acquire different imaging planes using a moving stage. Measurements took place in a temperature controlled water bath at 34 °C for acoustic coupling, and the samples were kept dry using a thin clear polyethylene membrane attached to the sample holder. We note that more recent versions of this system utilise 256 element arrays and up to 270° mouse coverage, however this system was not available during the original phase of the studies herein.

Animal imaging was performed under anaesthesia using 1.8% isoflurane in oxygen. Data were acquired along the animal, typically acquiring cross-sectional images at one position in the liver region, one position in the kidney region, and throughout the tumour when applicable using 1 mm steps. For animal imaging, 20 averages were acquired per wavelength at 680, 710, 740, 770, 800, 830, 860 and 900 nm. Images were acquired before liposomal injection and after intravascular tail-vein injection of 200  $\mu$ l of liposomes. Post-injection images were acquired at different time points at 5 min, 4 h and 24 h. We note that measurements acquired before liposomal injection were not used as baseline measurements but as control measurements, to examine possible cross-talk of the spectral unmixing method employed to indicate presence of liposomes.

### 3. Results and discussion

The expression of MUC-1 antigen in 4T1 murine breast and HT-29 human colon cell lines was validated by testing the binding capacity of hCTM01 anti-MUC-1 Ab alone after 3 h incubation at 37 °C using 1 µg/ml and 5 µg/ml Ab concentration. Immunostaining with Cy3-labelled secondary antibody and visualisation with confocal microscopy (Fig. 1) was used to examine hCTM01 Ab binding affinity and internalisation into 4T1 and HT-29 cells. Both 4T1 and HT-29 proved to have positive expression of MUC-1 antigen indication by the clear binding and internalisation of hCTM01 Ab. However, anti-MUC1 antigen expression was different between the two cell-lines. This can be seen from the higher binding affinity of HT-29 cells to hCTM01 Ab compared to 4T1 cells.

PEGylated liposome-ICG formulation was prepared using the lipid film hydration method followed by freeze-fracture cycles and extrusion, protocol previously described (Beziere et al., 2015). To engineer the targeted PEGylated liposome-ICG, we followed the previously reported post-insertion method that is based on the translocation of DSPE-PEG<sub>2000</sub>-Ab micellar lipids into pre-formed liposomal bilayers (Moreira et al., 2002). Briefly, hCTM01 was first conjugated to DSPE-PEG<sub>2000</sub>-Maleimide micelles followed by post-insertion into the pre-formed PEGylated liposome-ICG (Fig. 2A). In

this way, the Ab ligand will be presented at the outer surface of the liposomes and maintain its binding capacity (Sofou and Sgouros, 2008). The quantification of the monoclonal antibody hCTM01 conjugated to the liposomes was assessed by using the BCA assay combined to the Stewart assay for the lipid quantification at different eluted fractions after purification in Sepharose CL-4B (Fig. 2B). The amount of Ab conjugation was found to be 14% of the monoclonal antibody used (150 µg) in the eluted fractions 4–6 which contain 92% of the liposomes.

To elucidate the optical properties of the novel targeted liposome-ICG engineered, the optical density (OD) overtime was studied (Fig. 2C). The optical signal intensity at 810 nm performed over 5 days remained almost constant for both targeted and non-targeted liposomes. In order to exclude any possible effect of post-insertion process on the optical stability of the systems, non-targeted PEGylated liposome-ICG was included as a control. To allow direct comparison, both targeted and non-targeted PEGylated liposome-ICG were prepared following the same steps, except for the post-insertion process where HBS (pH 7.4) was used instead of mal-PEG<sub>2000</sub> Ab micelles.

The characterisation of PEGylated liposome-ICG before post-insertion and after post-insertion process for both targeted and non-targeted systems were assessed by measuring the lipid concentration using the Stewart assay and ICG quantification by

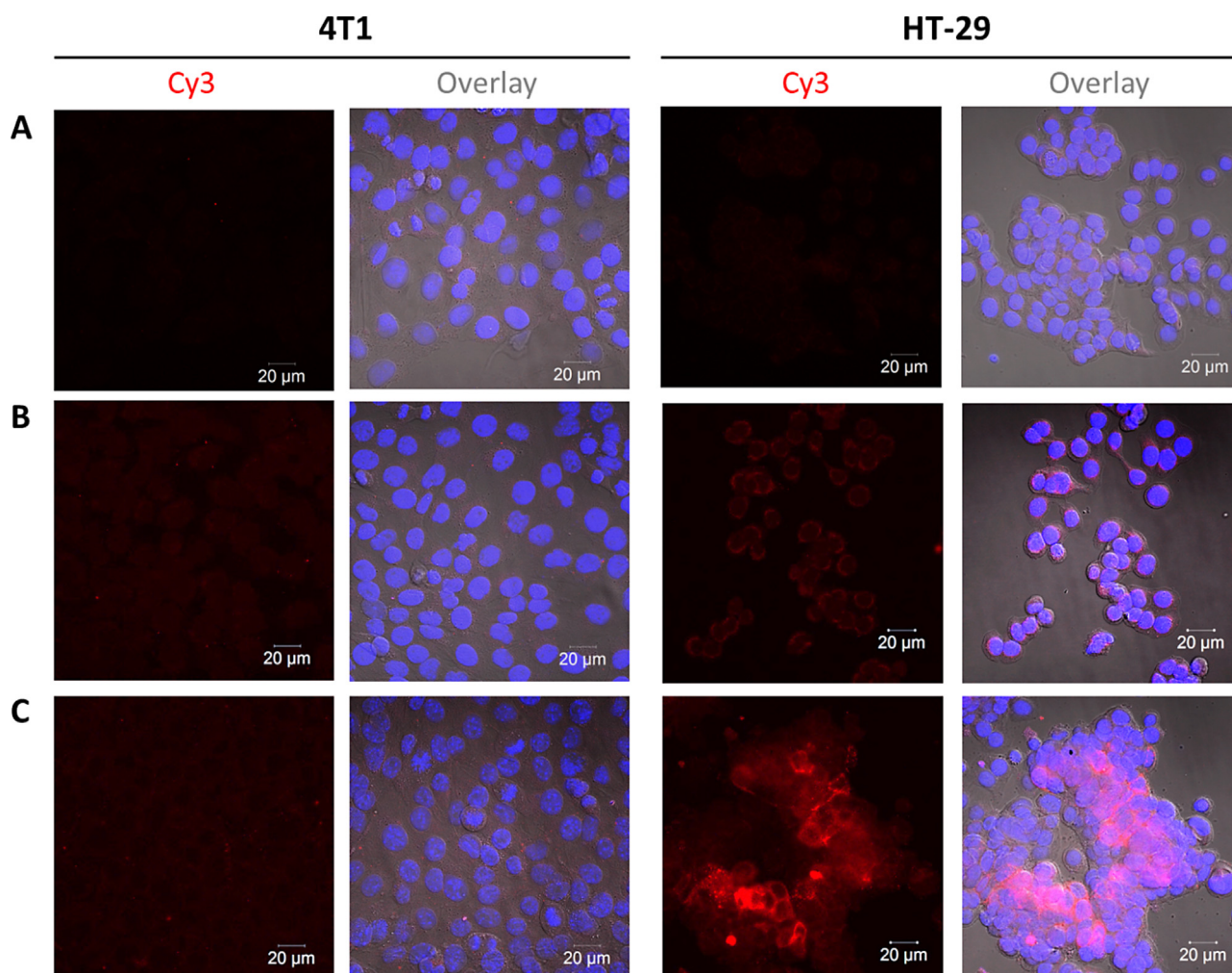


**Fig. 1.** Confocal images of 4T1 murine breast cell line and HT-29 colon adenocarcinoma cell line (MUC1 +) after 3 h incubation with (A) Ab free cell culture medium, (B) 1 µg/ml and (C) 5 µg/ml of hCTM01 Ab. After incubation with hCTM01 Ab cells were washed and stained with Cy3-labelled secondary antibody and imaged with CLSM. Red channel represents Cy3-labelled secondary antibody. Co-localization with DAPI stain (blue channel) of the nucleus is shown in the overlay images. Scale bar is 20 µm. (For interpretation of the references to colour in this figure legend, the reader is referred to the web version of this article.)

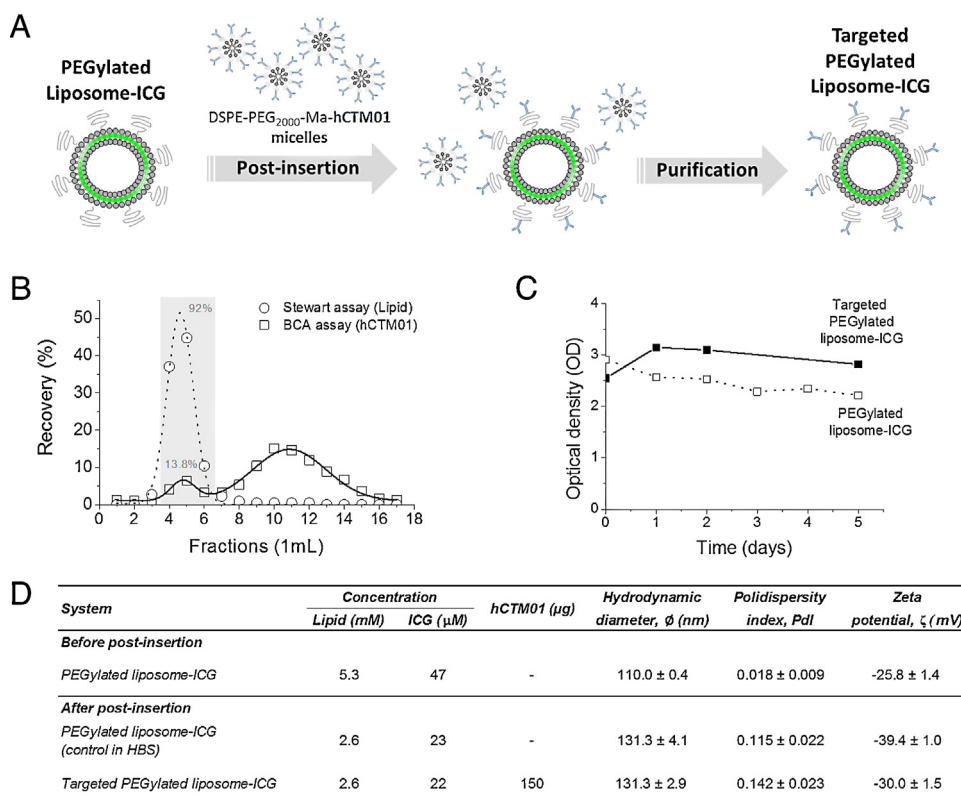


**Fig. 2.** Engineering of DSPE-PEG<sub>2000</sub>-maleimide-hCTM01 incorporation onto PEGylated liposome-ICG. (A) Schematic depiction of the post-insertion of the monoclonal antibody hCTM01-conjugated to DSPE-PEG<sub>2000</sub>-Maleimide micelles into the preformed PEGylated liposome-ICG in 5% dextrose. (B) Percentage of lipid recovery by using Stewart assay (circles) and percentage of antibody hCTM01 recovery by using the BCA assay (squares) for the 18 fractions of 1 ml eluted after Sepharose CL-4B purification. (C) Optical density (OD) at 810 nm for the targeted (solid line) and non-targeted (dashed line) PEGylated liposome-ICG. (D) Summary of the physico-chemical characterization of the targeted and non-targeted PEGylated liposome-ICG before and after post-insertion.

UV at 780nm wavelength after breaking the liposomes with DMSO. In addition, the amount of antibody conjugation was also quantified with BCA assay and hydrodynamic diameter ( $\phi$ ), polydispersity index (Pdl) and  $\zeta$ -potential were measure using the Malvern Zetasizer instrument (Fig. 2D). Both targeted and non-targeted PEGylated liposome-ICG contained almost the same amount of ICG after post-insertion so the conjugation of hCTM01 Ab did not affect the ICG incorporation into the liposomes. The hydrodynamic diameter increased from 110 to 130 nm for both systems after post-insertion but still within the suitable range to be intravenous administration for evaluation with MSOT imaging. The  $\zeta$ -potential became slightly more negative for both post-inserted liposomes in agreement with other previous studies (Chen, 2011; Yang et al., 2012).

To evaluate the tumour distribution of the targeted and non-targeted PEGylated liposome-ICG in HT-29 human colon adenocarcinoma (slow growth) and 4T1 murine breast tumour (fast growth), *in vivo* MSOT imaging was used (Fig. 3). For the pre-injection images, the cross-sectional anatomical images through the mouse at the tumour area were acquired at 800 nm as an anatomical guidance. MSOT images obtained from the 4T1 and HT-29 animal models after intravenous injection of both liposomes were shown in colour superimposed on anatomical cross-sectional images of the mouse obtained at 800 nm and plotted in grey scale. The presence of liposome-ICG on the MSOT images is identified based on its absorption spectrum after spectral unmixing of MSOT images obtained at multiple wavelengths as explained in the methods. Both liposomes provided an intense signal congruent with vascular structures identified on the anatomical image within the first minutes after injection. This is consistent with the previously reported pharmacokinetic profile of PEGylated

liposomes (Al-Jamal et al., 2012) and indicated that both liposomes at the early time points post-administration remained confined within the vascular system and did not localise within other tissues or deoxygenated regions of limited blood supply. Preferential accumulation was observed for the 4T1 tumour model, known for its faster growth compare to HT-29, regardless the presence of the antibody. However, the targeted liposomes accumulated faster at early time points. The non-targeted PEGylated liposomes accumulated in the centre of the tumour at later time points while a more diffuse tissue distribution in the periphery of the tumour and decrease of visible signal in the vasculature was observed for targeted liposomes. These observations indicated the potential of liposome-ICG in combination with MSOT live-imaging to provide non-invasively a better understanding of liposomal cancer treatment efficacy. We would also like to emphasize here on the effective role of hCTM01 antibody to improve the microdistribution of liposomes after accumulation into the tumour compared to non-targeted liposomes.

Taking this a step further, we encapsulated the anticancer drug, doxorubicin (DOX) into both targeted and non-targeted PEGylated liposome-ICG in order to combine both therapy and diagnosis. As described earlier in the Method section, DOX was encapsulated in the hydration step at the same time of ICG incorporation. Fig. 4A showed the post-insertion scheme of the PEGylated liposome-ICG-DOX with the DSPE-PEG<sub>2000</sub>-Ma-hCTM01 micelles. DOX encapsulation into both targeted and non-targeted liposome-ICG did not affect hCTM01 Ab conjugation to liposomes. The amount of monoclonal antibody hCTM01 conjugation was 11.6%, practically similar to what observed from the liposomes without DOX (Fig. 4B). The optical density of non-targeted PEGylated liposome-ICG encapsulated with DOX was higher than the targeted

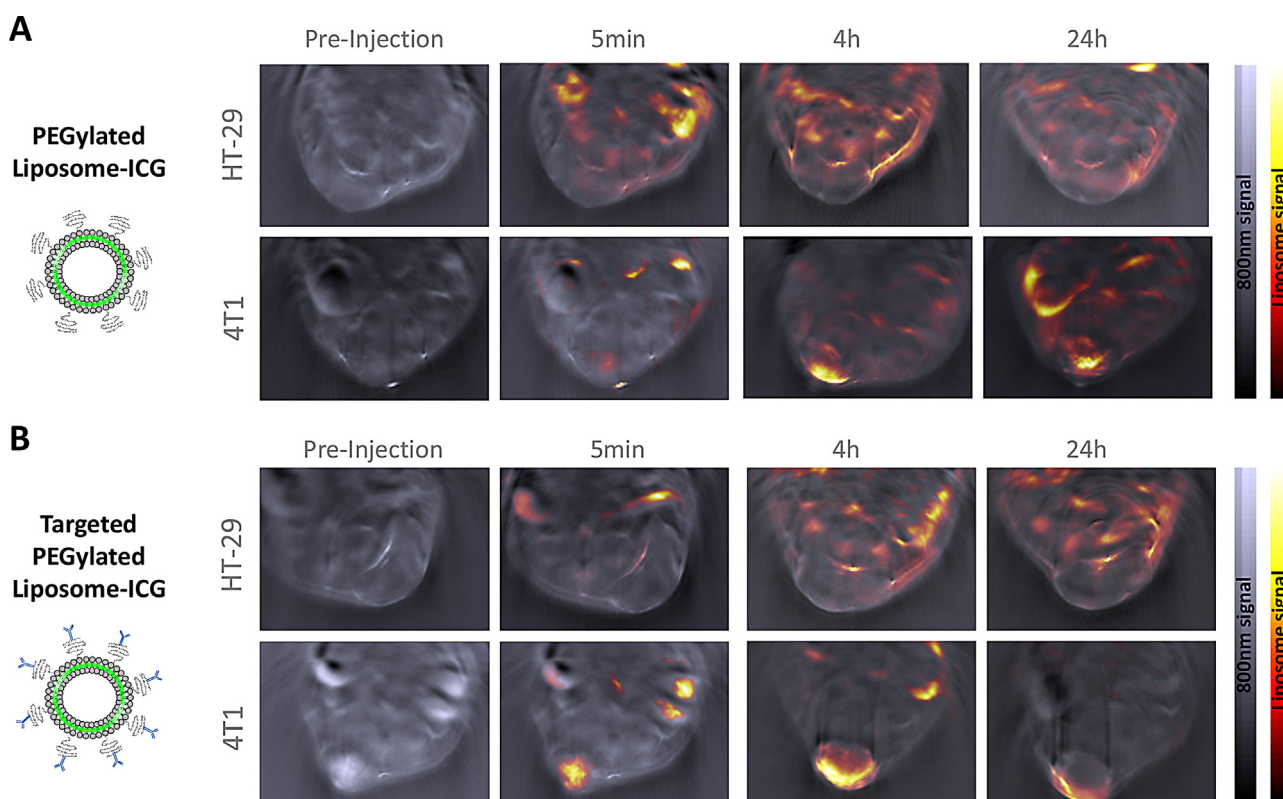


**Fig. 3.** *In vivo* MSOT imaging for HT-29 human colon and 4T1 murine breast tumour models after intravenous injection of the non-targeted and targeted PEGylated liposome-ICG. Liposome signal (hot scale) overlaid on single wavelength illumination images (800 nm, grey scale).

system with the drug (Fig. 4C). This difference in the optical density between targeted and targeted systems was not observed for the liposomes without DOX. In spite of this difference, the optical density remained constant for both systems over the time tested (5 days). In general, a noticeable increase in the size of PEGylated liposome-ICG was observed with DOX encapsulation compared to empty ones. (Fig. 4D). Similar to liposomes without DOX a slight increase in size was also observed after post insertion process for both targeted and non-targeted PEGylated liposome-ICG-DOX. Similar to systems studied without drug, slightly-ve  $\zeta$ -potential was detected after DOX encapsulation. Intra-tumoural distribution of targeted DOX loaded PEGylated liposome-ICG was then evaluated in 4T1 murine breast tumour bearing mice *in vivo* using MSOT live imaging (Fig. 4E). 4T1 tumour model was selected for this study as it showed higher tumour accumulation of liposome-ICG compared to HT-29 tumour model. MSOT images showed similar tumoural distribution of DOX-loaded targeted PEGylated liposome-ICG into 4T1 tumour model compared to those without DOX. As early as 5 min after intravenous injection ICG signal was able to be detected in the vasculature of the tumour. However, after prolonged time points (4 h and 24 h), a reduction in ICG signal in the vasculature was observed with higher localised homogenous tumour accumulation.

Significant progress has been made in the area of both passive and active drug targeting to tumours both at the preclinical and at the clinical level. Although such technologies have improved the understanding of the pathological and physiological principles of drug targeting to tumours, it has also identified several important pitfalls in this area (Lammers, 2012). Among those is the inadequate exploitation of non-invasive imaging techniques that could allow personalised medical treatment. An important issue in the field of tumour drug targeting that has been underestimated is that tumour animal models used in pre-clinical studies may not

represent adequately the clinical situation. This discrepancy between the pre-clinical and clinical situation is due to many factors, among them the difference in tumour growth rate, vascularity and different immune responses between animal models and humans. Therefore, combining diagnosis with therapy through theranostics drug design is thought to offer more valuable information for prediction and measurement of therapeutic responses that could facilitate their translation to the clinic (Lammers, 2012). Liposomal drug delivery systems are highly suitable for this purpose as they offer a modular platform, able to be adapted in a facile manner and incorporate imaging (Lozano et al., 2012) and therapeutic agents (Tejada-Berges et al., 2002).

Indeed image-guided delivery systems have been proved to be highly effective in the evaluation of tissue distribution and efficacy in tumour-specific drug delivery. Examples of that are Indium-111 radiolabelled PEGylated liposomes (Harrington et al., 2000) and MR image-guided thermosensitive liposomes co-encapsulating [Gd(HPDO3A)(H<sub>2</sub>O)] and doxorubicin (de Smet et al., 2013). Similarly, we have shown previously that ICG-labelled PEGylated liposomes in combination with MSOT can allow for highly effective non-invasive optical imaging, able to monitor liposomal tumour accumulation more accurately (Beziere et al., 2015). To improve the binding specificity and add a therapeutic functionality to this system, an active targeting moiety (hCTM01 Ab) and an anticancer drug (DOX) were incorporated into PEGylated liposome-ICG vesicles.

Targeted liposomes were shown to be effective in increasing cellular uptake, cytotoxicity and improve the intra-tumoural liposomal distribution even if the overall accumulation did not increase (Kirpotin et al., 2006; Lopes de Menezes et al., 1998; Lukyanov et al., 2004). In agreement with these studies, targeted PEGylated liposome-ICG vesicles developed in this work showed homogenous tumour distribution in the tumour mass compared to

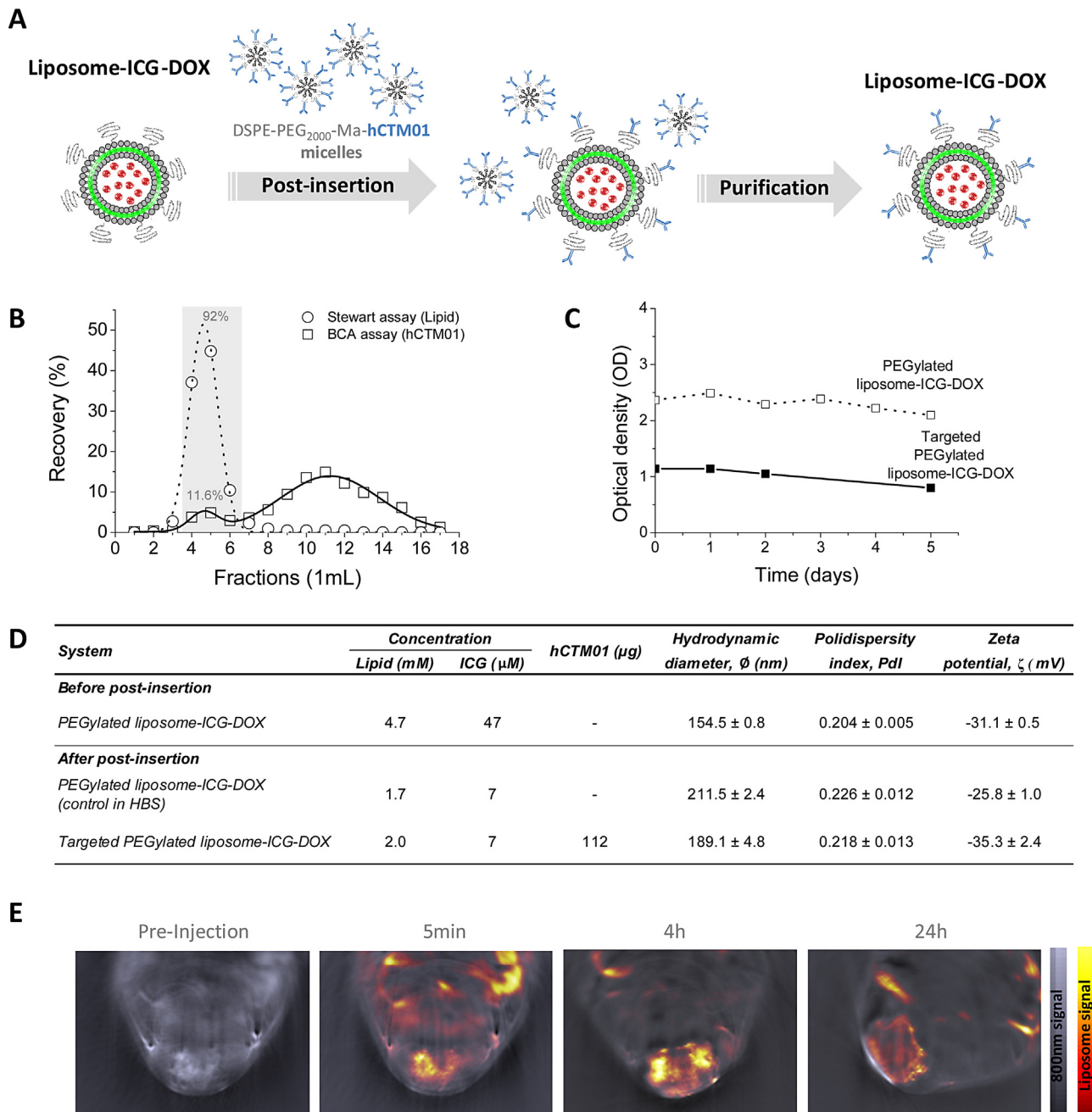


**Fig. 4.** Engineering, characterisation and MSOT imaging of monoclonal antibody (hCTM01)targeted PEGylated liposome-ICG-DOX vesicles. (A) Schematic depiction of the post-insertion of the monoclonal antibody hCTM01-conjugated to DSPE-PEG<sub>2000</sub>-Maleimide micelles into the preformed PEGylated liposome-ICG-DOX in 5% dextrose. (B) Percentage of lipid recovery by using Stewart assay (circles) and percentage of antibody hCTM01 recovery by using the BCA assay (squares) for the 18 fractions of 1 ml eluted after Sepharose CL-4B purification. (C) Optical density (OD) at 800 nm for the targeted (solid line) and non-targeted (dashed line) PEGylated liposome-ICG-DOX. (D) Summary of the physico-chemical characterization of the targeted and non-targeted PEGylated liposome-ICG-DOX before and after post-insertion. (E) *In vivo* MSOT imaging for 4T1 murine breast tumour model after intravenous injection of targeted PEGylated liposome-ICG-DOX. Liposome signal (hot scale) overlaid on single wavelength illumination images (800 nm, grey scale).

non-targeted vesicles that was not affected by DOX encapsulation. Similar to other *ex vivo* liposomal tumour accumulation quantification techniques (Al-Jamal et al., 2012), ICG-labelled liposomes with and without Ab coupled with MSOT imaging allowed both immediate and long-term detection of liposomes in the tumour. In addition, the differences in tumour mass accumulation and spatial distribution between targeted and non-targeted PEGylated liposome-ICG vesicles were observed between the two tumour models. MSOT imaging was able to reveal that such differences were mainly determined by the variability in growth rates and vascularisation among these tumour models. MoAb-targeting of

liposomes was not able to enhance significantly the accumulation within the HT-29 tumours that were not vascularised enough. However, in the case of the highly vascular 4T-1 model, more rapid accumulation was observed with the targeted systems. Encouragingly, remote-loading of DOX within such liposomes is feasible, albeit the low concentration of therapeutic agent encapsulated. Further work is under development in our laboratories to increase this to therapeutic doses.

The advantage of the vesicle system proposed in this study is the combination of non-invasive, high-resolution optoacoustic imaging (*via* the ICG component) and specific receptor-targeting

(via the hCTM01 surface conjugation) functionalities that are considered highly advantageous for both pre-clinical and clinical studies. In addition, the biocompatibility of both targeted and non-targeted PEGylated liposome-ICG systems and their long-term optical stability can facilitate their clinical translation. Systems like the ones described here, could certainly offer great advantage in the clinical setting to help identify which tumours are suitable for passive or active drug targeting and thereby predict which patients will be more likely to respond or not to treatment. In addition they could allow non-invasive follow-up after treatment by measurement of tumour volumes.

In conclusion, this study demonstrated the successful engineering of a monoclonal antibody-targeted PEGylated liposome-ICG system containing doxorubicin as a potential theranostic anticancer drug delivery system. Using this system in combination with MSOT imaging allowed the non-invasive monitoring in real-time of the vesicle tumour accumulation. Combination of technologies in this manner can open new insights into personalised therapeutics using image-guided theranostics.

### Conflict of interest

V.N. is a shareholder of iThera Medical GmbH.

### Acknowledgments

This research work was partially funded by the Andalusian Initiative for Advanced Therapies by the Regional Government of Andalusia, Spain (to N.L.) and the European Commission FP7 Program SONODRUGS (NMP4-LA-2008-213706) (to Z.A.). The authors would like to thank the Cluster of Excellence “Nanosystem Initiative Munich” and the ERC Advanced Grant (233161) “Next generation *in vivo* imaging platform for post-genome biology and medicine MSOT” for their financial support.

### References

- Al-Ahmady, Z.S., Chaloin, O., Kostarelos, K., 2014. Monoclonal antibody-targeted, temperature-sensitive liposomes: *in vivo* tumor chemotherapeutics in combination with mild hyperthermia. *J. Controlled Release* doi:http://dx.doi.org/10.1016/j.jconrel.2014.10.013.
- Al-Jamal, W.T., Al-Ahmady, Z.S., Kostarelos, K., 2012. Pharmacokinetics and tissue distribution of temperature-sensitive liposomal doxorubicin in tumor-bearing mice triggered with mild hyperthermia. *Biomaterials* 33, 4608–4617.
- Al-Jamal, W.T., Kostarelos, K., 2011. Liposomes: from a clinically established drug delivery system to a nanoparticle platform for theranostic nanomedicine. *Acc. Chem. Res.* 44, 1094–1104.
- Allen, T.M., 2002. Ligand-targeted therapeutics in anticancer therapy. *Nat. Rev. Cancer* 2, 750–763.
- Bangham, A.D., Horne, R.W., 1964. Negative staining of phospholipids and their structural modification by surface-active agents as observed in the electron microscope. *J. Mol. Biol.* 8, 660–668.
- Bao, C., Beziere, N., del Pino, P., Pelaz, B., Estrada, G., Tian, F., Ntziachristos, V., de la Fuente, J.M., Cui, D., 2013. Gold nanoprisms as optoacoustic signal nano-amplifiers for *in vivo* bioimaging of gastrointestinal cancers. *Small* 9, 68–74.
- Barenholz, Y., 2012. Doxil(R) – the first FDA-approved nano-drug: lessons learned. *J. Controlled Release* 160, 117–134.
- Beziere, N., Lozano, N., Nunes, A., Salichs, J., Queiros, D., Kostarelos, K., Ntziachristos, V., 2015. Dynamic Imaging of PEGylated indocyanine green (ICG) liposomes within the tumor microenvironment using multi-spectral optoacoustic tomography (MSOT). *Biomaterials* 37, 415–424.
- Buehler, A., Herzog, E., Razansky, D., Ntziachristos, V., 2010. Video rate optoacoustic tomography of mouse kidney perfusion. *Optics Lett.* 35, 2475–2477.
- Chan, S.Y., Gordon, A.N., Coleman, R.E., Hall, J.B., Berger, M.S., Sherman, M.L., Eten, C. B., Finkler, N.J., 2003. A phase 2 study of the cytotoxic immunoconjugate CMB-401 (hCTM01-calicheamicin) in patients with platinum-sensitive recurrent epithelial ovarian carcinoma. *Cancer Immunol. Immunother.* 52, 243–248.
- Chen, C.-W., 2011. Novel RGD-lipid conjugate-modified liposomes for enhancing siRNA delivery in human retinal pigment epithelial cells. *Int. J. Nanomed.* 6, 2567–2580.
- Davies, Q., Perkins, A.C., Frier, M., Watson, S., Lalani, E., Symonds, E.M., 1997. The effect of circulating antigen on the biodistribution of the engineered human antibody hCTM01 in a nude mice model. *Eur. J. Nucl. Med.* 24, 206–209.
- de Smet, M., Langereis, S., van den Bosch, S., Bitter, K., Hijnen, N.M., Heijman, E., Grull, H., 2013. SPECT/CT imaging of temperature-sensitive liposomes for MR-image guided drug delivery with high intensity focused ultrasound. *J. Controlled Release* 169, 82–90.
- Eitan, R., Fishman, A., Meirovitz, M., Goldenberg, H., Amit, A., Koren, C., Schneider, Y., Rosengarten, O., Neuman, A., Keren-Rosenberg, S., Safra, T., 2014. Liposome-encapsulated doxorubicin citrate (Myocet) for treatment of recurrent epithelial ovarian cancer: a retrospective analysis. *Anticancer Drugs* 25, 101–105.
- Fang, J., Nakamura, H., Maeda, H., 2011. The EPR effect: unique features of tumor blood vessels for drug delivery, factors involved, and limitations and augmentation of the effect. *Adv. Drug Delivery Rev.* 63, 136–151.
- Gabizon, A., Catane, R., Uziely, B., Kaufman, B., Safra, T., Cohen, R., Martin, F., Huang, A., Barenholz, Y., 1994. Prolonged circulation time and enhanced accumulation in malignant exudates of doxorubicin encapsulated in polyethylene-glycol coated liposomes. *Cancer Res.* 54, 987–992.
- Gabizon, A., Shmeeda, H., Grenader, T., 2012. Pharmacological basis of pegylated liposomal doxorubicin: impact on cancer therapy. *Eur. J. Pharm. Sci.* 45, 388–398.
- Gabizon, A., Tzemach, D., Gorin, J., Mak, L., Amitay, Y., Shmeeda, H., Zalipsky, S., 2010. Improved therapeutic activity of folate-targeted liposomal doxorubicin in folate receptor-expressing tumor models. *Cancer Chemother. Pharmacol.* 66, 43–52.
- Gillespie, A.M., Broadhead, T.J., Chan, S.Y., Owen, J., Farnsworth, A.P., Sopwith, M., Coleman, R.E., 2000. Phase I open study of the effects of ascending doses of the cytotoxic immunoconjugate CMB-401 (hCTM01-calicheamicin) in patients with epithelial ovarian cancer. *Ann. Oncol.* 11, 735–741.
- Harrington, K.J., Rowlinson-Busza, G., Syrigos, K.N., Vile, R.G., Uster, P.S., Peters, A.M., Stewart, J.S., 2000. Pegylated liposome-encapsulated doxorubicin and cisplatin enhance the effect of radiotherapy in a tumor xenograft model. *Clin. Cancer Res.* 6, 4939–4949.
- Herzog, E., Taruttis, A., Beziere, N., Lutich, A.A., Razansky, D., Ntziachristos, V., 2012. Optical imaging of cancer heterogeneity with multispectral optoacoustic tomography. *Radiology* 263, 461–468.
- Hinman, L.M., Hamann, P.R., Wallace, R., Menendez, A.T., Durr, F.E., Upeslacijs, J., 1993. Preparation and characterization of monoclonal antibody conjugates of the calicheamicins: a novel and potent family of antitumor antibiotics. *Cancer Res.* 53, 3336–3342.
- Iyer, A.K., Khaled, G., Fang, J., Maeda, H., 2006. Exploiting the enhanced permeability and retention effect for tumor targeting. *Drug Disc. Today* 11, 812–818.
- Jain, R.K., Stylianopoulos, T., 2010. Delivering nanomedicine to solid tumors. *Nat. Rev. Clin. Oncol.* 7, 653–664.
- Jeong, H.S., Lee, C.M., Cheong, S.J., Kim, E.M., Hwang, H., Na, K.S., Lim, S.T., Sohn, M.H., Jeong, H.J., 2013. The effect of mannosylation of liposome-encapsulated indocyanine green on imaging of sentinel lymph node. *J. Liposome Res.* 23, 291–297.
- Kirpotin, D.B., Drummond, D.C., Shao, Y., Shalaby, M.R., Hong, K., Nielsen, U.B., Marks, J.D., Benz, C.C., Park, J.W., 2006. Antibody targeting of long-circulating lipidic nanoparticles does not increase tumor localization but does increase internalization in animal models. *Cancer Res.* 66, 6732–6740.
- Lammers, T., 2012. Drug targeting to tumors: principles, pitfalls and (pre-) clinical progress. *J. Controlled Release* 161, 175–187.
- Loomis, K., Smith, B., Feng, Y., Garg, H., Yavlovich, A., Campbell-Massa, R., Dimitrov, D.S., Blumenthal, R., Xiao, X., Puri, A., 2010. Specific targeting to B cells by lipid-based nanoparticles conjugated with a novel CD22-ScFv. *Exp. Mol. Pathol.* 88, 238–249.
- Lopes de Menezes, D.E., Pilarski, L.M., Allen, T.M., 1998. *In vitro* and *in vivo* targeting of immunoliposomal doxorubicin to human B-cell lymphoma. *Cancer Res.* 58, 3320–3330.
- Lozano, N., Al-Jamal, W.T., Taruttis, A., Beziere, N., Burton, N.C., Van den Bossche, J., Mazza, M., Herzog, E., Ntziachristos, V., Kostarelos, K., 2012. Liposome-gold nanorod hybrids for high-resolution visualization deep in tissues. *J. Am. Chem. Soc.* 134, 13256–13258.
- Lukyanov, A.N., Elbayoumi, T.A., Chakilam, A.R., Torchilin, V.P., 2004. Tumor-targeted liposomes: doxorubicin-loaded long-circulating liposomes modified with anti-cancer antibody. *J. Controlled Release* 100, 135–144.
- Maeda, H., 2012. Vascular permeability in cancer and infection as related to macromolecular drug delivery, with emphasis on the EPR effect for tumor-selective drug targeting. *Proc. Jpn. Acad. Ser. B Phys. Biol. Sci.* 88, 53–71.
- Maeda, H., Nakamura, H., Fang, J., 2013. The EPR effect for macromolecular drug delivery to solid tumors: improvement of tumor uptake, lowering of systemic toxicity, and distinct tumor imaging *in vivo*. *Adv. Drug Delivery Rev.* 65, 71–79.
- Mamot, C., Drummond, D.C., Noble, C.O., Kallab, V., Guo, Z., Hong, K., Kirpotin, D.B., Park, J.W., 2005. Epidermal growth factor receptor – targeted immunoliposomes significantly enhance the efficacy of multiple anticancer drugs *in vivo*. *Cancer Res.* 65, 11631–11638.
- Minisini, A.M., Andretta, C., Fasola, G., Puglisi, F., 2008. Pegylated liposomal doxorubicin in elderly patients with metastatic breast cancer. *Expert Rev. Anticancer Ther.* 8, 331–342.
- Moreira, J.N., Ishida, T., Gaspar, R., Allen, T.M., 2002. Use of the post-insertion technique to insert peptide ligands into pre-formed stealth liposomes with retention of binding activity and cytotoxicity. *Pharm. Res.* 19, 265–269.
- Ntziachristos, V., Razansky, D., 2010. Molecular imaging by means of multispectral optoacoustic tomography (MSOT). *Chem. Rev.* 110, 2783–2794.
- Park, J.W., Kirpotin, D.B., Hong, K., Shalaby, R., Shao, Y., Nielsen, U.B., Marks, J.D., Papahadjopoulos, D., Benz, C.C., 2001. Tumor targeting using anti-her2 immunoliposomes. *J. Controlled Release* 74, 95–113.
- Prabhakar, U., Maeda, H., Jain, R.K., Sevic-Muraca, E.M., Zamboni, W., Farokhzad, O. C., Barry, S.T., Gabizon, A., Grodzinski, P., Blakey, D.C., 2013. Challenges and key

- considerations of the enhanced permeability and retention effect for nano-medicine drug delivery in oncology. *Cancer Res.* 73, 2412–2417.
- Prinssen, H.M., Molthoff, C.F., Verheijen, R.H., Broadhead, T.J., Kenemans, P., Roos, J. C., Davies, Q., van Hof, A.C., Frier, M., den Hollander, W., Wilhelm, A.J., Baker, T.S., Sopwith, M., Symonds, E.M., Perkins, A.C., 1998. Biodistribution of <sup>111</sup>In-labelled engineered human antibody CTM01 (hCTM01) in ovarian cancer patients: influence of prior administration of unlabelled hCTM01. *Cancer Immunol. Immunother.* 47, 39–46.
- Proulx, S.T., Luciani, P., Derzsi, S., Rinderknecht, M., Mumprecht, V., Leroux, J.C., Detmar, M., 2010. Quantitative imaging of lymphatic function with liposomal indocyanine green. *Cancer Res.* 70, 7053–7062.
- Sapra, P., Allen, T.M., 2002. Internalizing antibodies are necessary for improved therapeutic efficacy of antibody-targeted liposomal drugs. *Cancer Res.* 62, 7190–7194.
- Sawant, R.R., Torchilin, V.P., 2010. Liposomes as 'smart' pharmaceutical nano-carriers. *Soft Matter* 6, 4026–4044.
- Schwendener, R.A., Schott, H., 2010. Liposome formulations of hydrophobic drugs. *Methods Mol. Biol.* 605, 129–138.
- Sofou, S., Sgouros, G., 2008. Antibody-targeted liposomes in cancer therapy and imaging. *Expert Opin. Drug Delivery* 5, 189–204.
- Suzuki, R., Takizawa, T., Kuwata, Y., Mutoh, M., Ishiguro, N., Utoguchi, N., Shinohara, A., Eriguchi, M., Yanagie, H., Maruyama, K., 2008. Effective anti-tumor activity of oxaliplatin encapsulated in transferrin-PEG-liposome. *Int. J. Pharm.* 346, 143–150.
- Tejada-Berges, T., Granai, C.O., Gordinier, M., Gajewski, W., 2002. Caelyx/doxil for the treatment of metastatic ovarian and breast cancer. *Expert Rev. Anticancer Ther.* 2, 143–150.
- Torchilin, V., 2008. Antibody-modified liposomes for cancer chemotherapy. *Expert Opin. Drug Delivery* 5, 1003–1025.
- Yang, F.Y., Wang, H.E., Liu, R.S., Teng, M.C., Li, J.J., Lu, M., Wei, M.C., Wong, T.T., 2012. Pharmacokinetic analysis of <sup>111</sup>In-labeled liposomal doxorubicin in murine glioblastoma after blood–brain barrier disruption by focused ultrasound. *PLoS One* 7, e45468.
- Yang, T., Choi, M.-K., Cui, F.-D., Kim, J.S., Chung, S.-J., Shim, C.-K., Kim, D.-D., 2007. Preparation and evaluation of paclitaxel-loaded PEGylated immunoliposome. *J. Controlled Release* 120, 169–177.
- Zhuang, Y., Ma, Y., Wang, C., Hai, L., Yan, C., Zhang, Y., Liu, F., Cai, L., 2012. PEGylated cationic liposomes robustly augment vaccine-induced immune responses: role of lymphatic trafficking and biodistribution. *J. Controlled Release* 159, 135–142.